Temperature dependence of Al0.2Ga0.8As X-ray photodiodes for X-ray spectroscopy

Article (Published Version)

Temperature dependence of $Al_{0.2}Ga_{0.8}As$ X-ray photodiodes for X-ray spectroscopy

M. D. C. Whitaker, S. Butera, G. Lioliou, and A. M. Barnett

Citation: Journal of Applied Physics **122**, 034501 (2017); doi: 10.1063/1.4993914
View online: http://dx.doi.org/10.1063/1.4993914
View Table of Contents: http://aip.scitation.org/toc/jap/122/3
Published by the American Institute of Physics

Temperature dependence of $Al_{0.2}Ga_{0.8}As$ X-ray photodiodes for X-ray spectroscopy

M. D. C. Whitaker,[a] S. Butera, G. Lioliou, and A. M. Barnett
Semiconductor Materials and Devices Laboratory, School of Engineering and Informatics, University of Sussex, Falmer, Brighton BN1 9QT, United Kingdom

(Received 17 May 2017; accepted 1 July 2017; published online 17 July 2017)

Two custom-made $Al_{0.2}Ga_{0.8}As$ p^+-i-n^+ mesa X-ray photodiodes (200 μm diameter, 3 μm i layer) have been electrically characterised across the temperature range −20 °C to 60 °C. The devices were connected to a custom-made charge sensitive preamplifier to produce an AlGaAs photon-counting X-ray spectrometer. The devices' responses to illumination with soft X-rays from an ^{55}Fe radioisotope X-ray source (Mn Kα = 5.9 keV; Mn Kβ = 6.49 keV) were investigated across the temperature range −20 °C to 20 °C. The best energy resolution (FWHM at 5.9 keV) achieved at 20 °C was 1.06 keV (with the detector at 10 V reverse bias). Improved FWHM was observed with the devices at temperatures of 0 °C (0.86 keV) and −20 °C (0.83 keV) with the photodiode reverse biased at 30 V. The average electron hole pair creation energy was experimentally measured and determined to be 4.43 eV ± 0.09 eV at 20 °C, 4.44 eV ± 0.10 eV at 0 °C, and 4.56 eV ± 0.10 eV at −20 °C. *Published by AIP Publishing*. [http://dx.doi.org/10.1063/1.4993914]

I. INTRODUCTION

Wide bandgap materials, such as GaAs,[1–5] SiC,[6–8] diamond,[9,10] $Al_{0.52}In_{0.48}P$,[11–13] and $Al_xGa_{1-x}As$,[14–16] are of interest for use in space science and extreme terrestrial applications where detectors are exposed to high temperatures and intense radiation. Traditional Si X-ray spectrometers often require significant shielding and cooling mechanisms in order to function within extreme environments (e.g., ≫20 °C), whereas wide bandgap detectors are more robust and can possess superior energy resolution at high temperatures due to lower thermally induced leakage currents.[6] $Al_xGa_{1-x}As$ has received particular attention as a promising alternative for X-ray[14–16] and beta particle[17,18] detection; the material can be grown nearly lattice matched to readily available GaAs substrates, and by varying the Al concentration, the bandgap can be adjusted in order to meet specific application needs. The benefits exhibited by $Al_xGa_{1-x}As$ have led to the extensive study of $Al_{0.8}Ga_{0.2}As$ (i.e., higher Al composition than the present devices) for X-ray detection, where 200 μm diameter $Al_{0.8}Ga_{0.2}As$ circular mesa p^+-i-n^+ photodiodes with 1 μm i layers were characterised as soft X-ray photon counting detectors, with an energy resolution (FWHM) of 1.07 keV at 5.9 keV at room temperature for the best performing diode.[19] Larger devices (400 μm) with thicker epilayers (1.7 μm) and a similar structure to Ref. 19 have been reported with a mean leakage current density of 4.72 nA cm^{-2} ± 1.67 nA cm^{-2} at an average electric field strength of 29.4 kV/cm (5 V operating reverse bias), and a mean energy resolution (FWHM) of 1.27 keV at 5.9 keV at room temperature.[15] In addition to high Al concentrations (e.g., $Al_{0.8}Ga_{0.2}As$), $Al_{0.2}Ga_{0.8}As$ has also been preliminarily studied for X-ray detection at room temperature; three $Al_{0.2}Ga_{0.8}As$ p^+-i-n^+ mesa X-ray photodiodes (200 μm diameter, 3 μm i layer) were characterised for their response to soft X-ray illumination.[20]

In this article, extensive characterisation (including temperature dependence measurements) of two $Al_{0.2}Ga_{0.8}As$ p^+-i-n^+ mesa X-ray photodiodes is presented. The devices were grown and fabricated to the Authors' specifications at the EPSRC National Centre for III-V Technologies, Sheffield, UK.

II. DIODE DESIGN

The $Al_{0.2}Ga_{0.8}As$ p^+-i-n^+ mesa X-ray photodiode (200 μm diameter, 3 μm i layer) wafer was grown by metal-organic vapour phase epitaxy (MOVPE) on a commercial 2 in. GaAs n^+ substrate. The layer details are summarised in Table I. Circular mesa structures (200 μm diameter) were formed using a 1:1:1 H_3PO_4:H_2O_2:H_2O solution followed by 10 s in a 1:8:80 H_2SO_4:H_2O_2:H_2O solution. An Ohmic contact, consisting of 20 nm InGe and 200 nm Au, was evaporated onto the rear substrate, and an Ohmic top contact of 20 nm Ti and 200 nm Au was evaporated onto the p^+ side of the mesa devices; the top contact covered 45% of the diode's faces. The devices were unpassivated.

III. EXPERIMENTAL RESULTS

A. Capacitance as a function of applied bias

Capacitance as a function of applied forward and reverse bias was measured for the two $Al_{0.2}Ga_{0.8}As$ p^+-i-n^+ photodiodes D1 and D2, across the temperature range 60 °C to −20 °C, using an HP 4275A LCR Meter (signal magnitude 50 mV rms; frequency 1 MHz) and a Keithley 6487 picoammeter/voltage source to bias the detectors. The test harness, in which the $Al_{0.2}Ga_{0.8}As$ package was installed, was placed within a TAS Micro MT climatic cabinet for temperature control, and a thermocouple appropriately positioned in order to monitor the temperature and ensure that thermal

[a]Author to whom correspondence should be addressed: M.Whitaker@sussex.ac.uk

TABLE I. Layer details of the $Al_{0.2}Ga_{0.8}As$ diode.

Material	Dopant	Dopant type	Thickness (nm)	Doping density (cm^{-3})
GaAs	Be	p	10	1×10^{19}
$Al_{0.2}Ga_{0.8}As$	Be	p	500	2×10^{18}
$Al_{0.2}Ga_{0.8}As$		i	3000	Undoped
$Al_{0.2}Ga_{0.8}As$	Si	n	1000	2×10^{18}
GaAs n^+ substrate				

equilibrium was reached between the climatic cabinet and the devices at each temperature. The test harness was initially purged with dry N_2, then sealed, and the climatic cabinet was shut. The climatic cabinet was continually purged with dry N_2 for the duration of the measurement in order to maintain a dry N_2 environment (<5% relative humidity) to eliminate any humidity related effects.[4] National Instruments LabVIEW software was used to automate the characterisation routine. The temperature was initially set to 60 °C, and then decreased in 20 °C steps to −20 °C. The diodes were left for 30 min after reaching each temperature before measuring, to ensure thermal equilibrium and stabilisation. Figure 1 presents the capacitance as a function of applied forward bias at each measured temperature for the $Al_{0.2}Ga_{0.8}As$ p^+-i-n^+ photodiode, D1; comparable results were found for D2. Since the devices were measured after packaging, the capacitance of the package was removed by measuring the capacitance of an empty connection on the same package across the same applied bias range, and at each temperature, with each packaging capacitance value deducted from the respective total capacitance obtained for the detectors. This procedure also removes any additional unknown capacitances of the system, with the exception of the capacitance of the bond wires of each detector; however, subsequent analysis suggests that the bond wire capacitances were negligible compared with the other associated capacitances. Temperatures greater than 60 °C were not measured due to the high leakage currents (>40 nA at 10 V at 80 °C) being observed at such temperatures.

As the temperature was decreased from 60 °C to −20 °C, the forward capacitance, which is proportional to the forward current, of both devices decreased at each applied forward bias. At low applied reverse biases, the

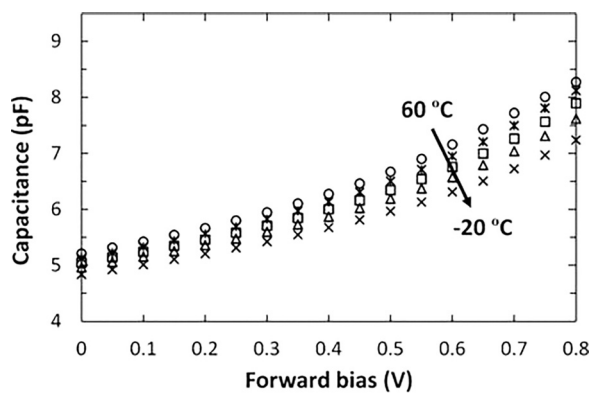

FIG. 1. Capacitance as a function of applied forward bias in the temperature range 60 °C to −20 °C, for D1; comparable results were obtained for D2.

measured capacitances decreased as the temperature decreased for both diodes: without application of reverse bias (i.e., 0 V), at 60 °C, capacitances of 5.20 pF ± 0.04 pF and 5.26 pF ± 0.04 pF were measured for D1 and D2, respectively; at −20 °C capacitances of 4.83 pF ± 0.04 pF and 4.90 pF ± 0.04 pF were measured. As the applied reverse bias was increased, the temperature dependence of the capacitance reduced, as shown in Fig. 2. At applied reverse bias ≥4 V, the variation in capacitance as a function of temperature became indiscernible i.e., the change in capacitance remained within the uncertainty of the measurement.

When reverse biased, the junction capacitance is predominantly defined by the depletion layer capacitance, $C_{DL}(V_R)$.[21] Thus, from the measured depletion layer capacitance $C_{DL}(V_R)$, the depletion width as a function of applied reverse bias $W(V_R)$ was calculated using

$$C_{DL}(V_R) = \frac{\varepsilon_0 \varepsilon A}{W(V_R)}, \quad (1)$$

where ε_0 is the permittivity of free space, ε is the relative permittivity of the material [12.332 for $Al_{0.2}Ga_{0.8}As$ (Ref. 22)], and A is the area of the device.[21] The depletion width of each diode increased as a function of applied reverse bias for all temperatures, until it reached an applied reverse bias of 30 V, where the measured depletion layer capacitance, and consequently the depletion width, remained constant, suggesting that the diodes were fully depleted at an applied reverse bias of 30 V (3.20 μm ± 0.15 μm and 3.01 μm ± 0.14 μm at −20 °C, 3.14 μm ± 0.14 μm, and 2.96 μm ± 0.13 μm at 60 °C, for D1 and D2 respectively, at an applied reverse bias of 30 V). The calculated depletion width as a function of applied reverse bias at −20 and 60 °C for diode D1 can be seen in Fig. 3. The depletion width of both diodes was found to be temperature independent, where the change in calculated depletion width

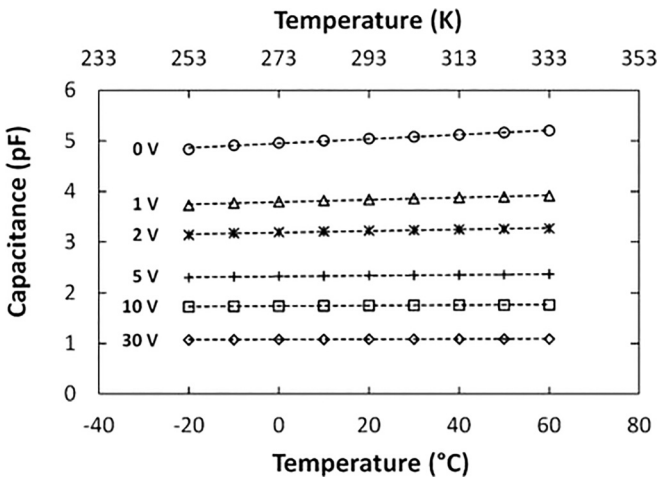

FIG. 2. Capacitance as a function of temperature for D1, in the temperature range −20 °C to 60 °C at six reverse bias values: 0 V (circles), 1 V (triangles), 2 V (stars), 5 V (plus signs), 10 V (squares), and 30 V (diamonds). The linear least squares fitting was applied to each data set in order to determine the capacitance per degree Celsius: (4.38 ± 0.18) fF °C^{-1} for 0 V, (2.24 ± 0.13) fF °C^{-1} for 1 V (1.51 ± 0.11) fF °C^{-1} for 2 V, (0.79 ± 0.07) fF °C^{-1} for 5 V, (0.47 ± 0.04) fF °C^{-1} for 10 V, and (0.24 ± 0.01) fF °C^{-1} for 30 V. Comparable results were obtained for D2, with calculated gradients falling within the uncertainty of those calculated for D1.

as a function of temperature lay within the measurement uncertainty.

The carrier concentration of the i layer, *N(W)*, was calculated using the equation for general nonuniform distributions[21]

$$\frac{d\left(1/C_{DL}^2\right)}{dV_R} = \frac{2}{q\varepsilon_0\varepsilon N(W)}, \tag{2}$$

where q is the elementary charge. The carrier concentration throughout the intrinsic region was calculated to be approximately $4.0 \times 10^{15}\,cm^{-3}$ and $4.4 \times 10^{15}\,cm^{-3}$ for D1 and D2, respectively. The variation of the carrier concentration, as a consequence of change in temperature, fell well within the calculated uncertainty of the measurement. At the i-n^+ interface, the carrier concentration increased to approximately $5 \times 10^{16}\,cm^{-3}$ for both D1 and D2. The carrier concentration as a function of distance, *W*, below the p^+-i junction for D1 has been plotted in Fig. 4.

B. Current measurements

Current, as a function of applied forward and reverse bias across the temperature range 60 °C to −20 °C, was measured using a Keithley 6487 Picoammeter/Voltage Source. The package and the associated diodes of interest (D1 and D2) were connected within a custom dark box, and installed within a TAS Micro MT climatic cabinet for temperature control. The custom dark box was initially purged with dry N_2, then sealed, and the climatic cabinet was shut. The climatic cabinet was continually purged with dry N_2 for the duration of the measurement in order to maintain a dry N_2 environment (<5% relative humidity) to eliminate any humidity related effects.[4] National Instruments LabVIEW software was used to automate the characterisation routine. The temperature was initially set to 60 °C and decreased in 20 °C increments to −20 °C, the minimum recorded temperature. The diodes were left to stabilise for 30 min at each temperature before measuring to ensure thermal equilibrium. Figure 5 presents the dark current as a function of applied forward bias for diode, D1, with dark current decreasing as a function of decreasing temperature. Comparable results were obtained for D2.

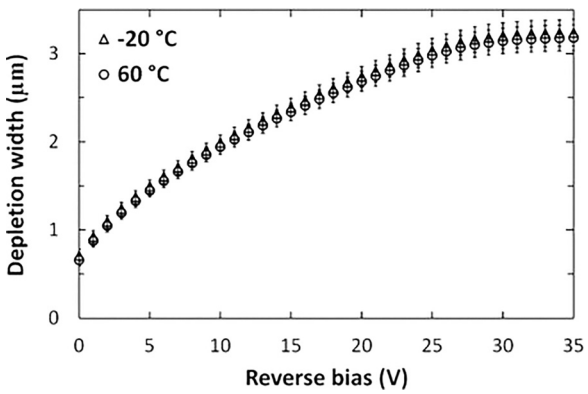

FIG. 3. Calculated depletion width as a function of reverse bias for D1, at −20 °C (triangles) and 60 °C (circles). Comparable results were obtained for D2.

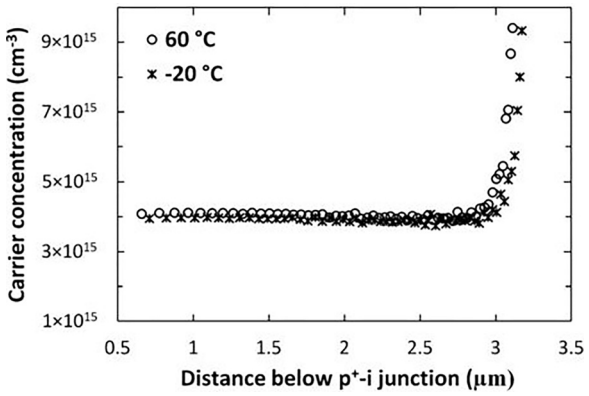

FIG. 4. Doping profile for D1, at 60 °C (circles) and −20 °C (stars). Comparable results were obtained for D2.

The forward current I_F, can be defined by the recombination current, I_{FR}, whose temperature dependence is

$$I_{FR} \propto n_i \exp\left(\frac{qV_F}{2kT}\right), \tag{3}$$

and the diffusion current, I_{FD}, whose temperature dependence is

$$I_{FD} \propto n_i^2 \exp\left(\frac{qV_F}{kT}\right), \tag{4}$$

where n_i is the intrinsic carrier concentration of the semiconductor material at a given temperature, *T*, k is the Boltzmann constant, and q is the charge of an electron.[4,21] Over the investigated temperature range, the forward current was found to be better described by Eq. (3) for both diodes, suggesting that recombination current is dominant. The saturation current, I_0, and the ideality factor, *n*, were calculated at each temperature, based on the linear region of the semi-logarithm I-V characteristics, as described in Refs. 4 and 23.

$$I_F = I_0 \exp\left(\frac{qV_F}{nkT}\right). \tag{5}$$

Equation (5) is valid only when $V_f > 3kT/q$, in addition, ideal diode behaviour was not exhibited until approximately

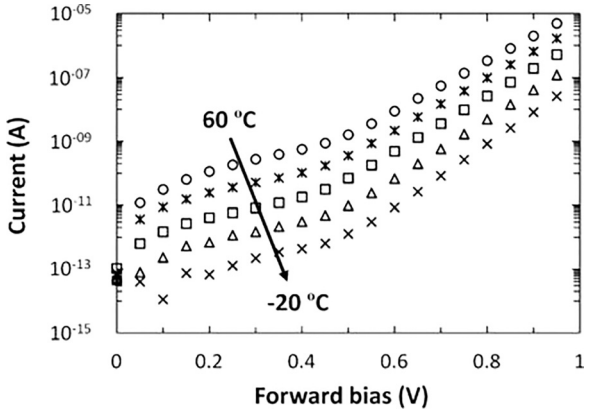

FIG. 5. Current as a function of applied forward bias in the temperature range 60 °C to −20 °C for D1. Comparable results were obtained for D2.

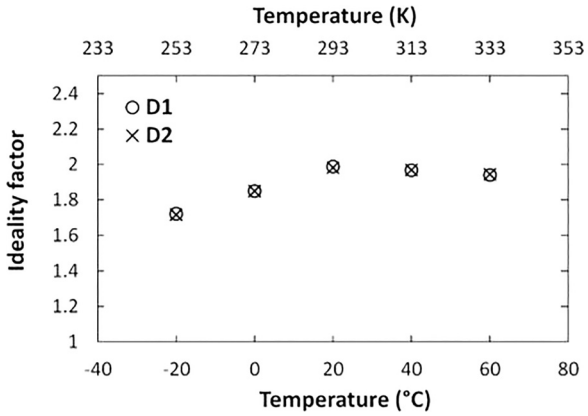

FIG. 6. Ideality factor as a function of temperature, extracted from the measured current as a function of applied forward bias ($0.65 \leq V_f \leq 0.95$) for D1 (circles) and D2 (crosses).

$V_f > 0.5$ V for both diodes, where at a lower applied forward bias, parallel resistances, or shunt resistance, is present. This shunt resistance is caused by defects, which can be in the form of diffusion paths along dislocations in the semiconductor, or leakage around the edge of the diode walls;[24] as a result, a linear least squares fit was applied to the region $0.65 \leq V_f \leq 0.95$. The saturation current was found to decrease as a function of decreasing temperature, from $(1.95 \pm 0.01) \times 10^{-13}$ A and $(1.99 \pm 0.01) \times 10^{-13}$ A at 60 °C, to $(8.70 \pm 0.03) \times 10^{-18}$ A and $(7.90 \pm 0.03) \times 10^{-18}$ A at −20 °C, for D1 and D2 respectively. Figure 6 presents the ideality factor as a function of temperature.

At room temperature (20 °C) and above, the ideality factor was ≈2 for D1 and D2. This suggests that recombination within the depletion region is the dominant limiting factor of current.[24] Below room temperature, however, the ideality factor decreased; this decrease suggests that fewer thermally stimulated crystal lattice defects are present within the detecting material when compared to room temperature and above.

The leakage current, I_r, as a function of applied reverse bias for D1 is shown in Fig. 7. The leakage current for both devices decreased as a function of decreasing temperature, where at the maximum applied reverse bias (30 V), the leakage current was measured to be $(3.00 \pm 0.01) \times 10^{-10}$ A at

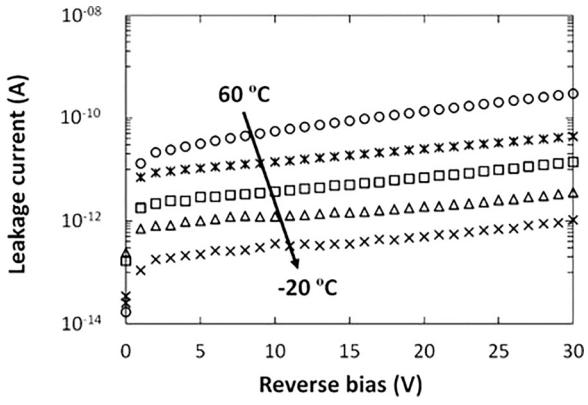

FIG. 7. Leakage current as a function of applied reverse bias in the temperature range 60 °C to −20 °C for D1. Comparable results were obtained for D2.

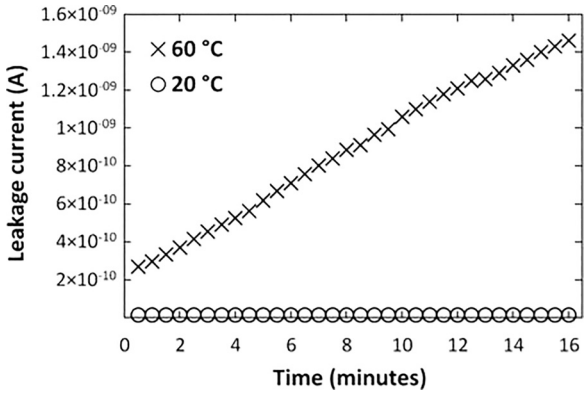

FIG. 8. Leakage current as a function of time for D1 at an applied reverse bias of 30 V and a temperature of 60 °C (crosses) and 20 °C (circles).

60 °C and $(1.05 \pm 0.40) \times 10^{-12}$ A at −20 °C for D1, and $(2.42 \pm 0.01) \times 10^{-10}$ A at 60 °C and $(9.98 \pm 4.03) \times 10^{-13}$ A at −20 °C for D2. Leakage current stability with time was also measured for both diodes, where the leakage current at the maximum applied reverse bias (30 V) was found to be stable at 20 °C and below, but not at hotter temperatures, as shown in Fig. 8.

Figure 9 presents the leakage current density at the maximum applied reverse bias (30 V, 100 kV/cm) as a function of temperature for D1. The leakage current density, J_R, increased exponentially with increasing temperature (−20 °C to 40 °C), however, beyond 40 °C, the trend changes, which suggests that the leakage current mechanism is different at higher temperatures.[4] Near identical results were obtained with D2, where the exponential fit coefficients over the temperature range −20 °C to 40 °C, were calculated to be $a = (1.11 \pm 0.02) \times 10^{-8}$ and $b = 0.063 \pm 0.001$. The leakage current density, J_R, can be expressed as

$$J_R = q{n_i}^2 \left(\frac{1}{N_d} \sqrt{\frac{D_p}{\tau_p}} + \frac{1}{N_a} \sqrt{\frac{D_n}{\tau_n}} \right) + q \frac{n_i}{2\tau_g} W, \qquad (6)$$

where N_d is the donor impurity concentration, N_a, is the acceptor impurity concentration, D_p and D_n are the hole and

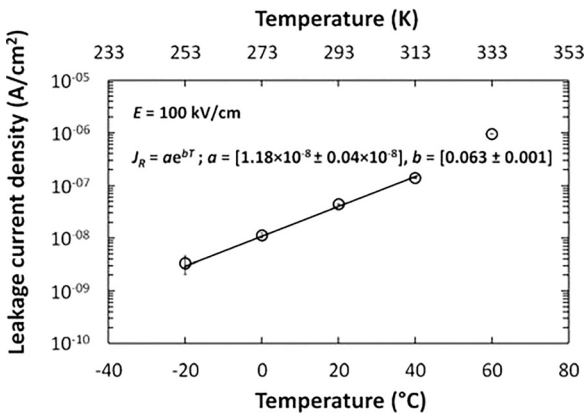

FIG. 9. Measured leakage current density, J_R, at a 100 kV/cm average internal electric field, E, as a function of temperature for D1. A linear least squares fitting has been applied with the line of best fit plotted.

electron diffusion coefficients respectively, τ_p and τ_n are the hole and electron carrier lifetimes respectively, τ_g is the carrier generation lifetime, and W is the depletion layer width.[4,25] The first and second term represent the diffusion and generation current respectively, where the diffusion current scales with n_i^2 and the generation current scales with n_i. Since

$$n_i^2 \propto \exp\left(-\frac{E_g}{kT}\right), \tag{7}$$

and

$$n_i \propto \exp\left(-\frac{E_g}{2kT}\right), \tag{8}$$

a plot of $\ln(J_R)$ as a function of $1/kT$ is expected to yield a straight line, whose slope determines the activation energy, E_A, and the dominant leakage current mechanism, where a gradient of $-E_g/2$, suggests that the generation current is dominant, and a gradient of E_g suggests that the diffusion current is dominant, where E_g is the bandgap energy.[4,21,25] Figure 10 shows $\ln(J_R)$ as a function of $1/kT$ plotted for D1.

Two linear regions ($E_A = -0.86$ eV; $E_A = -0.43$ eV $\pm$ 0.02 eV) are apparent in Fig. 10 which shows the data for D1. D2 exhibited comparable performance ($E_A = -0.79$ eV; $E_A = -0.43$ eV $\pm$ 0.02 eV) over the same ranges. Within the temperature range 40 °C to 60 °C, the slope was approximately $-E_g/2$ for both D1 and D2, where the bandgap (E_g) of $Al_{0.2}Ga_{0.8}As$ is 1.67 eV;[26] this corresponds to a generation dominant leakage current mechanism. Below 40 °C, the slope gradient was reduced (–0.43 eV). MBE growth of Be doped $Al_{0.2}Ga_{0.8}As$ p layers is known to cause 0.4 eV and 0.46 eV traps within the temperature ranges of 200–225 K and 250–300 K, respectively.[27,28] Since the temperature range (253.15–313.15 K), at which the slope of −0.43 eV was measured, resides within the trap temperature region, it is likely that this is responsible. At sufficiently high temperatures, diffusion current will always dominate,[25] therefore Fig. 10 suggests that the diffusion current must dominate at a temperature beyond 60 °C for the photodiodes measured.

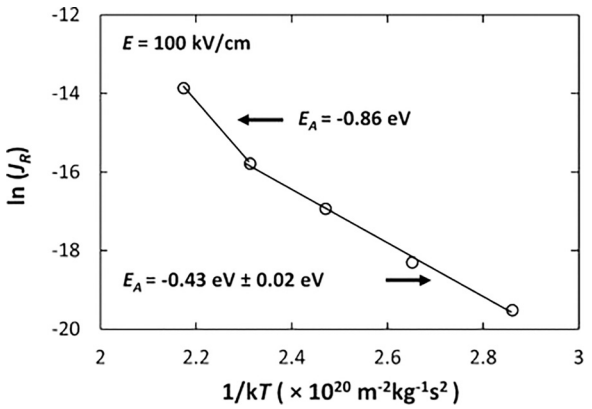

FIG. 10. Natural log of leakage current density, $\mathrm{Ln}(J_R)$, as a function of $1/kT$ at an average internal electric field, E, of 100 kV/cm for the $Al_{0.2}Ga_{0.8}As$ p^+-i-n^+ photodiode, D1. The linear least squares fitting was applied to the temperature ranges: 60 °C to 40 °C and 40 °C to −20 °C. The lines of best fit and respective activation energies (E_A) are shown.

Due to high leakage currents observed at temperatures greater than 60 °C, a higher temperature range was not investigated.

C. X-ray measurements

X-ray spectra were obtained using the $Al_{0.2}Ga_{0.8}As$ p^+-i-n^+ photodiode, D1, to characterise the X-ray detection performance as a function of temperature. The diode was connected to a custom-made low-noise charge-sensitive single channel preamplifier of feedback resistorless design similar to Ref. 29. The preamplifier used a Si JFET (2N4416A, capacitance ≈2 pF) as the input transistor. The preamplifier was connected to an Ortec 571A shaping amplifier (shaping time = 0.5 μs, the optimum for the system used) and an Ortec 927 ASPEC multi-channel analyser (MCA). An ^{55}Fe radioisotope X-ray source (193 MBq) emitting characteristic Mn Kα (5.9 keV) and Mn Kβ (6.49 keV) X-rays was placed 3 mm above the $Al_{0.2}Ga_{0.8}As$ p^+-i-n^+ photodiode, housed within the preamplifier. The detector along with the preamplifier, were installed inside a TAS Micro MT climatic cabinet throughout the measurements for temperature control, and a thermocouple placed close to the detecting system to ensure a temperature agreement between the climatic cabinet and the detecting system. The climatic cabinet was continually purged with dry N_2 (<5% relative humidity) in order to reduce humidity related effects.

The temperature was initially set to 20 °C, and was decreased to a minimum temperature of −20 °C, in steps of 20 °C, where the device was allowed to stabilise for 30 min upon reaching the desired temperature in order to ensure thermal equilibrium. A maximum temperature of 20 °C was set due to diode instability at greater temperatures over the time used to accumulate the spectra. Spectra were accumulated at each temperature, with the photodiode reverse biased at 0 V, 10 V, 20 V, and 30 V. The live time limit for each spectrum was 1000 s. Gaussian fitting was applied to the detected photopeak from the ^{55}Fe radioisotope X-ray source (Mn Kα = 5.9 keV; Mn Kβ = 6.49 keV), taking into account the relative emission ratio[30] and the relative efficiency of the detector at these respective energies. The spectra were energy calibrated using the positions of the zero energy noise peak and the fitted Mn Kα 5.9 keV peak, with the assumption of a linear variation of detected charge with energy. The impact ionization coefficients of $Al_{0.2}Ga_{0.8}As$, as a function of average internal electric field, were calculated and indicated that the diodes were operating within the non-avalanche regime. The FWHM was measured for all obtained spectra, and was plotted as a function of reverse bias in Fig. 11.

Room temperature device performance was found to be better than previously reported for $Al_{0.2}Ga_{0.8}As$ X-ray photodiodes at room temperature, where a FWHM at 5.9 keV of 1.24 keV was measured at an average internal electric field strength of 33 kV/cm. Using the presently reported devices, a FWHM at 5.9 keV = 1.06 keV was measured at the same applied electric field. Figure 12 shows spectra accumulated of the ^{55}Fe radioisotope X-ray source with the spectrometer at 20 °C and −20 °C at a detector applied reverse bias of 20 V, where the reduction of the FWHM due to decreasing

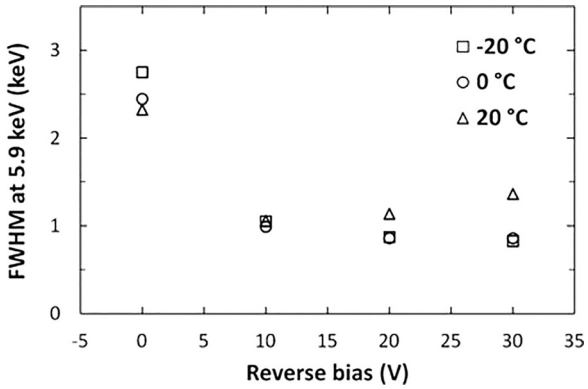

FIG. 11. Measured FWHM at 5.9 keV as a function of applied reverse bias for the $Al_{0.2}Ga_{0.8}As$ p^+-i-n^+ photodiode, D1, in the temperature range −20 °C to 20 °C at a shaping time of 0.5 μs.

temperature can be seen. The low energy tailing in the accumulated spectra was attributed to the partial collection of charge created by X-ray photons absorbed in the low-field regions of the photodiode/substrate.[15]

D. Noise analysis

The energy resolution of a non-avalanche semiconductor detector coupled to a charge sensitive preamplifier is influenced by three sources of noise:[31] the Fano noise, a consequence of the statistical nature of the X-ray absorption ionization process,[32] the electronic noise, arising from the detector and preamplifier electronics, and the incomplete charge collection noise (including charge trapping).[33] The fundamental Fano-limited energy resolution (FWHM) at 5.9 keV was calculated to be 131 eV for $Al_{0.2}Ga_{0.8}As$ at room temperature, assuming a Fano factor of 0.12 and an electron hole pair creation energy of 4.43 eV (see Sec. III E). Since the measured energy resolution of the system is greater than the calculated fundamental Fano-limited energy resolution, it was possible to conclude that a significant noise contribution from either the electronics noise, or incomplete charge collection noise, was present.

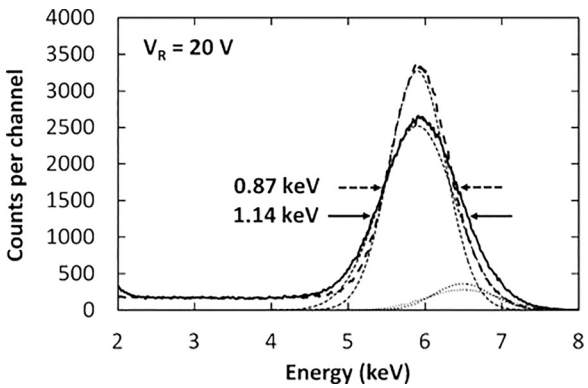

FIG. 12. ^{55}Fe spectra accumulated with the $Al_{0.2}Ga_{0.8}As$ p^+-i-n^+ photodiode D1 at a shaping time of 0.5 μs and an applied reverse bias of 20 V at two operating temperatures: −20 °C (dashed line) and 20 °C (solid line). The Mn Kα (narrow dashed line) and Mn Kβ (dotted line) The Gaussian fitted peaks have also been plotted. The total number of counts under the Gaussian associated with the ^{55}Fe Mn Kα peak was ≈360 000 in each case.

The electronic noise consists of parallel white noise, series white noise, induced gate drain current noise, 1/*f* series noise, and dielectric noise.[15] Figure 13 presents the calculated values of these noise contributions, as per Refs. 34, 35, and 36. A more detailed explanation of the electronic noise contributions is given in Ref. 37.

The parallel white noise component is due to the leakage current of the detector and of the input Junction Field-Effect Transistor (JFET),[4] and was calculated based on the measured leakage current of the detector at different temperatures (Fig. 7) and on the estimated leakage current of the input JFET as a function of temperature.[38] The series white noise, due to the capacitance of the detector and the input JFET,[4] was calculated based on the measured capacitance of the detector at different temperatures (Fig. 2) and on the estimated input capacitance of the input JFET.[38] The known dielectric noise was calculated by taking the quadratic sum of the known individual dielectric noise of the detector and JFET. A quadratic sum of the noise components (series white noise, parallel white noise, 1/*f* series noise, the expected Fano noise, and the known dielectric noise) was subtracted from the total FWHM of the 5.9 keV photopeak, and was attributed to the unknown dielectric noise, and stray series white noise since incomplete charge collection noise has been previously shown to be insignificant in these devices in this operation condition.[20]

At no applied bias, the FWHM ranged from 2.33 keV at 20 °C to 2.75 keV at −20 °C. Since the quadratic sum of the known noise contributions with no applied bias decreased from 551 eV at 20 °C to 501 eV at −20 °C, the unknown dielectric noise, stray series white noise, and incomplete charge collection accounted for the increase in FWHM as the temperature was reduced (2.24 keV at 20 °C and 2.47 keV at −20 °C). The optimal operating reverse bias for the $Al_{0.2}Ga_{0.8}As$ detector was found to be 10 V at room temperature (1.06 keV FWHM at 5.9 keV), and 30 V for 0 °C (0.86 keV FWHM at 5.9 keV) and −20 °C (0.83 keV FWHM at 5.9 keV). The variation in operating bias dependence of the energy resolution as a function of

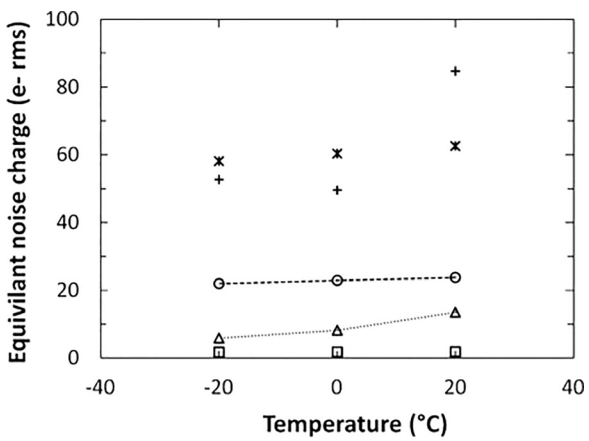

FIG. 13. Calculated remaining noise contributions of the $Al_{0.2}Ga_{0.8}As$ p^+-i-n^+ photodiode D1 at an applied reverse bias of 20 V and a shaping time of 0.5 μs as a function of temperature: combined unknown dielectric noise, incomplete charge collection noise, and any additional stray series white noise (plus signs); known dielectric noise (stars); series white noise (circles); parallel white noise (triangles); 1/*f* series noise (squares).

decreasing temperature is a result of the interplay between the noise driven by the detector's capacitance (series white noise) and the detector's leakage current (parallel white noise) contributions, where at 20 °C and at an applied reverse bias of 30 V, the increased parallel white noise (192 eV) relative to 10 V (108 eV), exceeds the benefits of a reduced series white noise contribution (232 eV) relative to an applied reverse bias of 10 V (283 eV). However, at lower temperatures (e.g., −20 °C), the reduction in parallel white noise (71 eV), relative to 10 V (58 eV), in addition to a lower series white noise contribution (215 eV) relative to 10 V (261 eV), reduces the FWHM at 5.9 keV accordingly (1.36 keV at 20 °C and 0.83 keV at −20 °C for an applied reverse bias of 30 V, and 1.06 keV at 20 °C and 1.05 keV at −20 °C for an applied reverse bias of 10 V).

E. Electron-hole pair creation energy measurements

The electron-hole pair creation energy, ε, at room temperature was determined for $Al_{0.2}Ga_{0.8}As$ relative to that of GaAs ($\varepsilon_{GaAs} = 4.184\,eV \pm 0.025\,eV$).[39] This method was previously used to determine ε in SiC[6] and GaAs[39] using a Si reference detector, and in $Al_{0.8}Ga_{0.2}As$ using a GaAs reference detector.[40] The well characterised[41] GaAs p^+-i-n^+ mesa X-ray photodiode (200 μm diameter, 10 μm i layer) structure is shown in Table II.

The two detectors ($Al_{0.2}Ga_{0.8}As$ D1 and the GaAs reference photodiode) were connected in parallel to the same readout electronics as used above. The detectors and preamplifier were kept at room temperature (20 °C) during the experiment. The ^{55}Fe radioisotope X-ray source was positioned above each detector in turn taking great care not to disturb any other aspect of the apparatus.[42] The live time limit for each spectrum was 1000 s. X-ray spectra were accumulated as a function of applied reverse bias (10 V, 15 V, and 20 V) of the $Al_{0.2}Ga_{0.8}As$ diode, D1, in order to ensure that no electric field dependencies (e.g., charge collection losses) affected the electron-hole pair creation energy results. The GaAs reference detector was kept at its optimum reverse bias of 10 V for each accumulated spectra. The shaping time of the shaping amplifier was set to 1 μs (the optimal shaping time for the dual detector configuration). The experimental system differs only slightly from that used in Refs. 6, 39, and 40, in that although the detectors were connected in parallel they were illuminated individually. This adjusted method was used in order to prevent any possible additional distortion (undershoot) within the preamplifier output caused as a consequence of two detectors being connected in parallel.[42] Although such an undershoot can typically be resolved by implementing a pole-zero cancellation,[42] the preamplifier response to the pulse would not be a simple exponential in this case, and consequently, it would be impractical to perform pole-zero cancellation in the amplifier.[42] Thus, the improved experimental method was used to eliminate the problem. Whilst obtaining measurements in this way can introduce the possibility of detector or input JFET leakage current instabilities over time, preliminary measurements of these parameters indicated that no such effects were present over the experiment's duration when the set up was operated in the described conditions, and thus they did not affect the measurements. Figure 14 presents the representative spectra obtained with the $Al_{0.2}Ga_{0.8}As$ and GaAs detectors when they were connected in parallel and illuminated separately; the spectra are presented within the same figure for the convenience of the reader. Charge calibration was achieved using the positions of the zero energy noise peak of the preamplifier and the 5.9 keV Mn Kα peak observed with the reference GaAs diode, together with the accepted ε_{GaAs} value. The dashed and dotted lines are the fitted Mn Kα peaks for the $Al_{0.2}Ga_{0.8}As$ and GaAs detectors, respectively.

Since the electron-hole pair creation energies of $Al_{0.2}Ga_{0.8}As$ and GaAs differ, so does the average number of charge carriers created by the absorption of a photon of energy E (Ref. 40) in each material (as shown by the different positions of the peaks' centroids in Fig. 14). As such, since previous investigation of the $Al_{0.2}Ga_{0.8}As$ detector and the GaAs reference detector have shown charge trapping to be negligible,[20,41] where a unity Charge Collection Efficiency (CCE = 1) can be assumed for both devices, the ratio of the average numbers of charge carriers (N_{AlGaAs} for $Al_{0.2}Ga_{0.8}As$ and N_{GaAs} for GaAs) created by the absorption of a photon of energy E, in conjunction with the known electron-hole pair creation energy of GaAs (ε_{GaAs}), can be used to determine ε_{AlGaAs}

$$\varepsilon_{AlGaAs} = \varepsilon_{GaAs}\left(\frac{N_{GaAs}}{N_{AlGaAs}}\right). \tag{9}$$

TABLE II. Layer details of the GaAs reference diode.

Material	Dopant	Dopant type	Thickness (nm)	Doping density (cm^{-3})
GaAs	Be	p	500	2×10^{18}
GaAs		i	10 000	Undoped
GaAs	Si	n	1000	2×10^{18}
GaAs n^+ substrate				

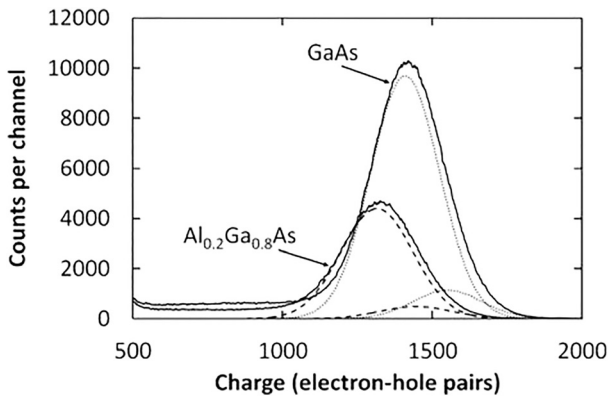

FIG. 14. Accumulated spectra at room temperature with an ^{55}Fe radioisotope X-ray source placed above the $Al_{0.2}Ga_{0.8}As$ detector, D1, (solid line as indicated) and the GaAs reference detector (solid line as indicated) at an applied reverse bias of 10 V and a shaping time of 1 μs. The detectors were connected in parallel but illuminated individually in turn; their spectra have been overlaid on the same calibrated charge scale. The Mn Kα and Mn Kβ Gaussian fitted peaks of the $Al_{0.2}Ga_{0.8}As$ detector (dashed lines), and the GaAs reference detector (dotted lines) have also been plotted.

The spectra obtained with the $Al_{0.2}Ga_{0.8}As$ and GaAs photodetectors were fitted with the Mn Kα (5.9 keV) and Mn Kβ (6.49 keV) peaks in the accepted ratio,[30] taking into account the detectors' relative detection efficiencies for the Mn Kα and Mn Kβ emissions, as shown in Fig. 14. The accepted value of ε_{GaAs} was then used in conjunction with Eq. (9) to calculate ε_{AlGaAs}. With the $Al_{0.2}Ga_{0.8}As$ detector biased at 10 V, 15 V, and 20 V, ε_{AlGaAs} was found to be $4.48\,eV \pm 0.09\,eV$, $4.42\,eV \pm 0.09\,eV$, and $4.40\,eV \pm 0.09\,eV$, respectively. All determined values were within the estimated uncertainties of each other. The mean of these measurements was $4.43\,eV \pm 0.09\,eV$, which agrees with the value predicted at room temperature when assuming a linear variation of ε with the Al fraction between GaAs(Ref. 39) and $Al_{0.8}Ga_{0.2}As$ (Ref. 17) (=4.4 eV).

Since ε_{AlGaAs} did not significantly reduce with the increasing reverse bias of the $Al_{0.2}Ga_{0.8}As$ device, the assumption that the determined value of ε_{AlGaAs} was not significantly influenced by charge trapping within the i-layer appears valid. Had charge losses been significant at low reverse biases, it would have been expected that at higher reverse biases, a significantly reduced value of ε_{AlGaAs} would have resulted. However, because complete charge collection within the i-layer cannot be absolutely guaranteed, the value of $4.43\,eV \pm 0.09\,eV$ should still be taken as an upper limit, which may decrease in future as a higher quality material is grown.[43]

The $Al_{0.2}Ga_{0.8}As$ electron-hole pair creation energy was then studied across the temperature range $-20\,^{\circ}C$ to $20\,^{\circ}C$. The GaAs reference detector was removed from the experimental setup, and thus the $Al_{0.2}Ga_{0.8}As$ p^+-i-n^+ photodiode, D1, was individually connected to a custom-made low-noise charge-sensitive preamplifier. The ^{55}Fe radioisotope X-ray source was positioned 3 mm above the $Al_{0.2}Ga_{0.8}As$ diode, and the detector and preamplifier were installed inside the TAS Micro MT climatic cabinet, and a thermocouple was also used in order to measure the temperature and ensure thermal equilibrium. The climatic cabinet was continually purged with dry N2 (<5% relative humidity) in order to reduce any humidity related effects. A stabilised pulse generator (Berkeley Nucleonic Corporation model BH-1) was connected to the test signal input of the custom preamplifier, such that the change in conversion factor of the preamplifier as a result of change in temperature could be measured, and its effects taken into account in the subsequent analysis.[43] The preamplifier was connected to the same shaping amplifier and MCA, as previously. Spectra were accumulated at each temperature, decreasing from $20\,^{\circ}C$ to $-20\,^{\circ}C$, in steps of $20\,^{\circ}C$. The photodiode was reverse biased to 0 V, 10 V, 20 V, and 30 V at each temperature, with a live time limit of 1,000 s and a shaping time of 0.5 μs (the optimal shaping time for this set up) set for each spectrum. For each spectrum, the photopeak was fitted with Gaussians corresponding to the Mn Kα and Kβ peaks, and the peak from the pulse generator. The positions of the peak centroids, with respect to the zero noise peak, were calculated. The relative change in position of the Mn Kα peak on the MCA's charge scale, taking into account the preamplifier's change in conversion factor with temperature (determined from the pulser peak) and the change in test capacitance as a function of temperature, enabled the determination of the change in the electron-hole pair creation energy of $Al_{0.2}Ga_{0.8}As$ with temperature.[43] Knowing the electron-hole pair creation energy for $Al_{0.2}Ga_{0.8}As$ at $20\,^{\circ}C$ ($4.43\,eV \pm 0.09\,eV$), enabled the calculation of the absolute value of the electron-hole pair creation energy at the other temperatures. Figure 15 presents the electron-hole pair creation energy as a function of temperature for $Al_{0.2}Ga_{0.8}As$.

For each applied reverse bias investigated, the average energy required to produce an electron-hole pair decreased with increasing temperature. Variations in the calculated electron-hole pair creation energy, as a function of reverse bias at each temperature, fell within the uncertainty of the measurement. A linear relationship between the electron-hole pair creation energy and temperature can be seen in Fig. 15, and has been evaluated using linear least squares fitting such that: $\varepsilon_{AlGaAs} = aT + b$, where $a = (-0.003 \pm 0.001)\ eV\ K^{-1}$ and $b = (5.403 \pm 0.395)\ eV$. The calculated gradient, defining the relationship between the electron-hole pair creation energy and temperature in $Al_{0.2}Ga_{0.8}As$, was found to be shallower than for $Al_{0.8}Ga_{0.8}As$ [$-0.0077\ eV\ K^{-1}$ (Ref. 43)], and steeper than for GaAs [$-0.00122\ eV\ K^{-1}$ (Ref. 39)], as expected.

The relationship between the electron-hole pair creation energy and the physical parameters of semiconductor materials has been subject to study using a variety of incident radiation types.[44] According to Klein,[45] the relationship between the electron-hole pair creation energy and the bandgap energy of a given semiconductor can be expressed as

$$\varepsilon\,[\mathrm{eV}] = \left(\frac{9}{5}\right)E_g + E_g + r(\hbar\omega_r), \tag{10}$$

where E_g is the intrinsic bandgap, (9/5) E_g is the residual kinetic energy, and $r(\hbar\omega_r)$ accounts for the optical phonon losses which, according to Klein, lies within the range $0.5 \le r(\hbar\omega_r) \le 1.0$ (eV).[45] The measured electron-hole pair creation energies of many materials and their associated bandgap energies was presented by Owens and Peacock,[33] and subsequently by Owens,[46] where a traditional "main"

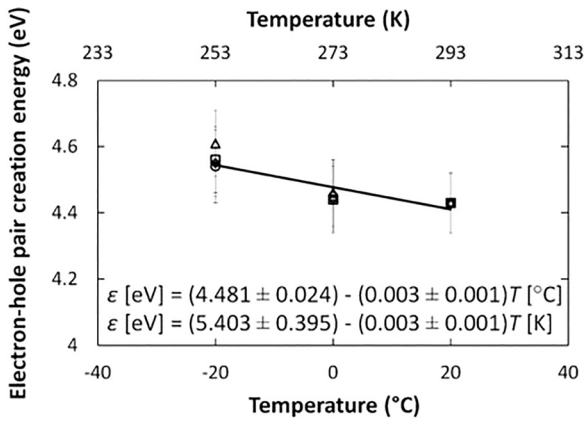

FIG. 15. The average energy required to produce an electron-hole pair in $Al_{0.2}Ga_{0.8}As$ at an applied reverse bias of 0 V (circles), 10 V (triangles), 20 V (squares), and 30 V (diamonds) as a function of temperature, with the line of best fit plotted.

Klein function branch ($\varepsilon = (14/5)E_g + 0.6$) was identified in the data set, along with a number of materials including diamond, AlN, 4H-SiC, PbI_2, and HgI_2, which were displaced from the main branch and lay on an apparent secondary Klein function branch, where $r(\hbar\omega_r) = -1.5$ eV, which was identified as unphysical within the Klein model.[33] Thus, as demonstrated by Owens and Peacock, the Klein relationship between the electron-hole pair creation and bandgap energy is unsatisfactory. Additionally, for the data compiled by Owens and Peacock, it is difficult to determine the temperatures at which the measurements of bandgap and electron-hole pair creation energy included in the Klein plots were made.[33] Since the electron-hole pair creation energy is a temperature dependent parameter, knowledge of the temperature at which the measurements were made is critical to the interpretation of the data. Likewise, the material qualities of many of the semiconductors, used to make the measurements, which were subsequently collated and summarised by Owens and Peacock, are also questionable in some cases.[33]

Considering only the well characterised materials Ge, Si, and GaAs, at room temperature, Bertuccio and Maiocchi[39] reported a linear relationship between bandgap and electron-hole pair creation energy which differed from the "main" and "secondary" Klein branches. Barnett *et al.*[40,43] subsequently extended this dataset with measurements for $Al_{0.8}Ga_{0.2}As$, refining the Bertuccio and Maiocchi linear fit, and additionally demonstrating that $Al_{0.8}Ga_{0.2}As$ fitted neither the main nor the secondary Klein branch.

The electron-hole pair creation energy measurements reported here show that $Al_{0.2}Ga_{0.8}As$ is another material that does not fit either of the Klein branches. If $Al_{0.2}Ga_{0.8}As$ was to lie on the main Klein function branch, a value of $\varepsilon = 5.28$ eV at room temperature would have been expected. If $Al_{0.2}Ga_{0.8}As$ was situated on the secondary Klein function branch, a value of $\varepsilon = 3.18$ eV at room temperature would have been expected. The measured value ($\varepsilon = 4.43$ eV $\pm$ 0.09 eV at room temperature) was between those predicted by the Klein functions. However, $\varepsilon = 4.43$ eV $\pm$ 0.09 eV for $Al_{0.2}Ga_{0.8}As$ is in remarkable agreement with the Bertuccio–Maiocchi–Barnett (BMB) relationship, which predicted $\varepsilon = 4.47$ eV $\pm$ 0.29 eV for $Al_{0.2}Ga_{0.8}As$. Refining the BMB relationship with the new experimental data for $Al_{0.2}Ga_{0.8}As$ yields a linear least squares fit, where at room temperature ε [eV] $= (1.58 \pm 0.09)\ E_g + (1.83 \pm 0.13)$, as shown in Fig. 16. This linear fit lies within the uncertainties calculated by Barnett *et al.*[43]

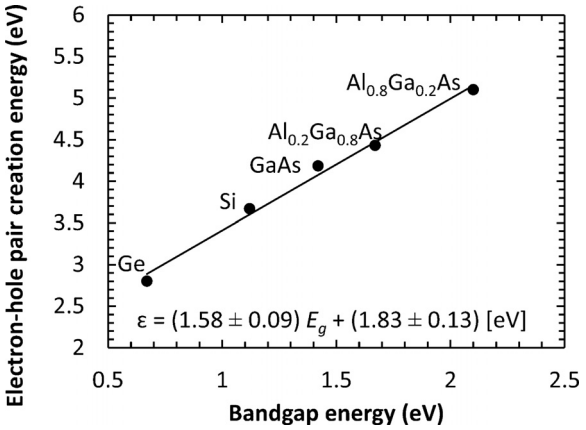

FIG. 16. Electron-hole pair creation energies for Ge, Si, GaAs, $Al_{0.2}Ga_{0.8}As$, and $Al_{0.8}Ga_{0.2}As$ plotted as a function of their respective bandgap energies at room temperature.

IV. DISCUSSION, CONCLUSIONS, AND FURTHER WORK

Two $Al_{0.2}Ga_{0.8}As$ p^+-i-n^+ mesa X-ray photodiodes (200 μm diameter, 3 μm i layer) have been electrically characterised across the temperature range 60 °C to −20 °C; in addition, one of the diodes has been characterised as a detector for photon counting X-ray spectroscopy across the temperature range from 20 °C to −20 °C, and the electron-hole pair creation energy is measured.

The ideality factor of the devices, as a function of temperature, was calculated based on the measured current as a function of applied forward bias, and was found to improve from (1.942 ± 0.001) and (1.946 ± 0.001) at 60 °C to (1.723 ± 0.001) and (1.719 ± 0.001) at −20 °C for D1 and D2 respectively. The calculated ideality factors indicated that recombination current defined the forward current, and such a small temperature dependence excluded tunnelling from significant contribution to the forward current.[4]

The leakage current for both devices decreased as a function of decreasing temperature. At the maximum applied reverse bias (30 V), the leakage current decreased from $(3.00 \pm 0.01) \times 10^{-10}$ A, (953.67 ± 4.13) nA cm^{-2} at 60 °C to $(1.05 \pm 0.40) \times 10^{-12}$ A, (3.35 ± 1.28) nA cm^{-2} at −20 °C for D1, and $(2.42 \pm 0.01) \times 10^{-10}$ A, (768.89 ± 3.58) nA cm^{-2} at 60 °C to $(9.98 \pm 4.03) \times 10^{-13}$ A, (3.18 ± 1.28) nA cm^{-2} at −20 °C for D2. The leakage current density was found to exponentially increase with temperature up to 40 °C, but at 60 °C, the leakage current density did not follow the expected trend, and was larger than expected for both investigated diodes; this was a consequence of the 0.4 eV and 0.46 eV traps within the Be doped $Al_{0.2}Ga_{0.8}As$ p layers as discussed in Sec. III B.

The capacitance, as a function of forward applied bias, increased with increasing temperature for both investigated diodes, which was found to be in agreement with current measurements as a function of forward bias, where an increase in current with increasing temperature was also observed.

Measurements of the depletion layer capacitance showed that, beyond an applied reverse bias of 4 V, the depletion layer capacitance was independent of temperature. At an applied reverse bias of 30 V, the measured depletion layer capacitance, and consequently the depletion width, remained constant, suggesting that the diodes were fully depleted. The i layer thickness was calculated to be 3.2 μm $\pm$ 0.2 μm and 3.0 μm $\pm$ 0.1 μm for D1 and D2 respectively. The carrier concentration, 2 μm below the p^+-i junction, was calculated to be 4×10^{15} cm^{-3} and 4.4×10^{15} cm^{-3} for D1 and D2, respectively. At the i-n^+ interface, the carrier concentration increased to 5×10^{16} cm^{-3} for both D1 and D2.

X-ray detection performance of D1 was characterised as a function of temperature from −20 °C to 20 °C. ^{55}Fe X-ray spectra were accumulated at a shaping time of 0.5 μs, and at

different operating reverse bias conditions (0 V, 10 V, 20 V, and 30 V). The best energy resolution (FWHM at 5.9 keV) at room temperature was obtained at an operating reverse bias of 10 V (1.06 keV FWHM at 5.9 keV), whilst the best energy resolution at 0 °C (0.86 keV FWHM at 5.9 keV) and −20 °C (0.83 keV FWHM at 5.9 keV) was achieved at a detector reverse bias of 30 V. The best previously reported energy resolution for non-avalanche AlGaAs X-ray detectors (200 μm diameter; 1 μm i layer) is 1.07 keV FWHM at 5.9 keV at room temperature;[19] the currently reported $Al_{0.2}Ga_{0.8}As$ p^+-i-n^+ mesa X-ray photodiode (200 μm diameter, 3 μm i layer) presented had comparable energy resolution at room temperature (1.06 keV FWHM at 5.9 keV). However, the reported energy resolution achieved is modest when compared with those recently measured using the state-of-the-art Silicon Drift Detectors (SDDs) coupled to state-of-the-art ultra-low-noise CMOS readout electronics, even at room temperature [FWHM = 141 eV at 5.9 keV (Ref. 47)].

The average energy consumed in the generation of an electron-hole pair in $Al_{0.2}Ga_{0.8}As$ has been experimentally measured at X-ray energies by measuring the charge created in $Al_{0.2}Ga_{0.8}As$ from an ^{55}Fe radioisotope X-ray source (Mn Kα = 5.9 keV, Mn Kβ = 6.49 keV). A value of $\varepsilon_{AlGaAs} = (4.43 \pm 0.09)$ eV was measured at room temperature. In the temperature range −20 °C to 20 °C, ε_{AlGaAs} was found to linearly decrease, from (4.56 ± 0.10) eV at −20 °C to (4.43 ± 0.09) eV at 20 °C, such that: $\varepsilon_{AlGaAs} = aT + b$, where $a = (-0.003 \pm 0.001)$ eV K^{-1} and $b = (5.403 \pm 0.395)$ eV.

In future work, characterisation of $Al_{0.2}Ga_{0.8}As$ detectors of different areas and thicknesses will be reported, as will characterisation of their response to illumination with X-ray photons of different energies. In order to revise the theory of the relationship between electron-hole pair creation energy and bandgap energy, we plan to continue the study of $Al_xGa_{1-x}As$ at varying x in order to map the dependence of electron-hole pair creation energy with bandgap energy across the GaAs to AlAs range, as well as conducting further measurements on these and other materials.

ACKNOWLEDGMENTS

This work was supported in part by the Science and Technology Facilities Council, UK, Grants ST/M004635/1 and ST/P001815/1. M.D.C.W. and G.L. each independently acknowledge funding received in the form of Ph.D. scholarships from the University of Sussex, UK. A.M.B. acknowledges funding from the Leverhulme Trust, UK, in the form of a 2016 Philip Leverhulme Prize. The authors are grateful to B. Harrison, R. J. Airey, and S. Kumar at the EPSRC National Centre for III-V Technologies for material growth and fabrication.

[1]A. Owens, M. Bavdaz, A. Peacock, A. Poelaert, H. Andersson, S. Nenonen, H. Sipila, L. Tröger, and G. Bertuccio, J. Appl. Phys. **90**, 5376 (2001).
[2]G. Bertuccio, R. Casiraghi, D. Maiocchi, A. Owens, M. Bavdaz, A. Peacock, H. Andersson, and S. Nenonen, IEEE Trans. Nucl. Sci. **50**, 723 (2003).
[3]A. M. Barnett, J. E. Lees, D. J. Bassford, J. S. Ng, C. H. Tan, N. Babazadeh, and R. B. Gomes, Nucl. Instrum. Methods Phys. Res., Sect. A **654**, 336 (2011).
[4]G. Lioliou, X. Meng, J. S. Ng, and A. M. Barnett, J. Appl. Phys. **119**, 124507 (2016).
[5]A. Owens, M. Bavdaz, A. Peacock, A. Poelaert, H. Andersson, S. Nenonen, L. Tröger, and G. Bertuccio, Nucl. Instrum. Methods Phys. Res., Sect. A **466**, 168 (2001).
[6]G. Bertuccio and R. Casiraghi, IEEE Trans. Nucl. Sci. **50**, 175 (2003).
[7]G. Bertuccio, S. Caccia, D. Puglisi, and D. Macera, Nucl. Instrum. Methods Phys. Res., Sect. A **652**, 193 (2011).
[8]S. Zhao, T. Gohil, G. Lioliou, and A. M. Barnett, Nucl. Instrum. Methods Phys. Res., Sect. A **830**, 1 (2016).
[9]H. Kagan, Nucl. Instrum. Methods Phys. Res., Sect. A **546**, 222 (2005).
[10]M. Zhang, Phys. Lett. A **332**, 320 (2004).
[11]A. Auckloo, J. S. Cheong, X. Meng, C. H. Tan, J. S. Ng, A. Krysa, R. C. Tozer, and J. P. R. David, J. Instrum. **11**, P03021 (2016).
[12]S. Butera, G. Lioliou, A. B. Krysa, and A. M. Barnett, J. Appl. Phys. **120**, 024502 (2016).
[13]S. Butera, T. Gohil, G. Lioliou, A. B. Krysa, and A. M. Barnett, J. Appl. Phys. **120**, 174503 (2016).
[14]J. Lauter, D. Protić, A. Förster, and H. Lüth, Nucl. Instrum. Methods Phys. Res., Sect. A **356**, 324 (1995).
[15]A. M. Barnett, G. Lioliou, and J. S. Ng, Nucl. Instrum. Methods Phys. Res., Sect. A **774**, 29 (2015).
[16]A. Silenas, J. Pozela, K. Pozela, L. Dapkus, and V. Juciene, Nucl. Instrum. Methods Phys. Res., Sect. A **563**, 21 (2006).
[17]A. M. Barnett, J. E. Lees, and D. J. Bassford, J. Instrum. **8**, P10014 (2013).
[18]A. Silenas, A. Miller, J. Pozela, K. Pozela, L. Dapkus, and V. Juciene, Nucl. Instrum. Methods Phys. Res., Sect. A **633**, S62 (2011).
[19]A. M. Barnett, D. J. Bassford, J. E. Lees, J. S. Ng, C. H. Tan, and J. P. R. David, Nucl. Instrum. Methods Phys. Res., Sect. A **621**, 453 (2010).
[20]M. D. C. Whitaker, G. Lioliou, S. Butera, and A. M. Barnett, Nucl. Instrum. Methods Phys. Res., Sect. A **840**, 168 (2016).
[21]S. M. Sze, *Physics of Semiconductor Devices*, 3rd ed. (John Wiley & Sons, New Jersey, 2006).
[22]S. Adachi, *Properties of Aluminium Gallium Arsenide* EMIS Data Reviews Series No. 7, INSPEC (The Institution of Electrical Engineers, London, 1993).
[23]A. Sellai, in *Proceedings of the IEEE International Conference on Semiconductor Electronics, Johor, Malaysia, 25 November–27 November 2008*, pp. 267–270.
[24]A. Luque, *Handbook of Photovoltaic Science and Engineering*, 2nd ed. (John Wiley & Sons, New Jersey, 2003).
[25]H. Spieler, *Semiconductor Detector Systems* (Oxford University Press, New York, 2005).
[26]L. Berger, *Semiconductor Materials* (CRC Press, Boca Raton, 1996).
[27]J. Szatkowski, E. Placzek-Popko, K. Sierański, and O. P. Hansen, J. Appl. Phys. **86**, 1433 (1999).
[28]R. H. Mari, M. Shafi, M. Aziz, A. Khatab, D. Taylor, and M. Henini, Nanoscale Res. Lett. **6**, 180 (2011).
[29]G. Bertuccio, P. Rehak, and D. Xi, Nucl. Instrum. Methods Phys. Res., Sect. A **326**, 71 (1993).
[30]U. Schötzig, Appl. Radiat. Isot. **53**, 469 (2000).
[31]G. W. Fraser, *X-Ray Detectors in Astronomy* (Cambridge University Press, Cambridge, 1989).
[32]G. Bertuccio, IEEE Solid State Circuits Mag. **4**, 36 (2012).
[33]A. Owens and A. Peacock, Nucl. Instrum. Methods Phys. Res., Sect. A **531**, 18 (2004).
[34]G. Bertuccio, A. Pullia, and G. De Geronimo, Nucl. Instrum. Methods Phys. Res., Sect. A **380**, 301 (1996).
[35]E. Gatti, P. F. Manfredi, M. Sampietro, and V. Speziali, Nucl. Instrum. Methods Phys. Res., Sect. A **297**, 467 (1990).
[36]A. M. Barnett, J. E. Lees, D. J. Bassford, and J. S. Ng, Nucl. Instrum. Methods Phys. Res., Sect. A **673**, 10 (2012).
[37]G. Lioliou and A. M. Barnett, Nucl. Instrum. Methods Phys. Res., Sect. A **801**, 63 (2015).
[38]Anon. *N-Channel JFETs: 2N4416* (Vishay Intertechnology Inc., USA, 2005).
[39]G. Bertuccio and D. Maiocchi, J. Appl. Phys. **92**, 1248 (2002).
[40]A. M. Barnett, J. E. Lees, and D. J. Bassford, J. Instrum. **7**, P06016 (2012).
[41]G. Lioliou and A. M. Barnett, Nucl. Instrum. Methods Phys. Res., Sect. A **836**, 37 (2016).
[42]An American National Standard, IEEE Standard Test Procedures for Amplifiers and Preamplifiers used with Detectors of Ionizing Radiation, 1989.

[43]A. M. Barnett, J. E. Lees, and D. J. Bassford, Appl. Phys. Lett. **102**, 181119 (2013).
[44]R. H. Pehl, F. S. Goulding, D. A. Landis, and M. Lenzlinger, Nucl. Instrum. Methods Phys. Res., Sect. A **59**, 45 (1968).
[45]C. A. Klein, J. Appl. Phys. **39**, 2029 (1968).
[46]A. Owens, *Compound Semiconductor Radiation Detectors* (CRC Press, Boca Raton, 2012).
[47]G. Bertuccio, M. Ahangarianabhari, C. Graziani, D. Macera, Y. Shi, A. Rachevski, I. Rashevskaya, A. Vacchi, G. Zampa, N. Zampa, P. Bellutti, G. Giacomini, A. Picciotto, and C. Piemonte, J. Instrum. **10**, P01002 (2015).